AGU PUBLICATIONS

JGR

Journal of Geophysical Research: Atmospheres

RESEARCH ARTICLE
10.1002/2014JD021790

Key Points:
- BC measured over 47 years at Kevo, Finland, in the Arctic showed a 78% decrease
- Ore smelting in Kola Peninsula significantly contributed to BC at Kevo
- Model calculations estimate BC that was nearly 4X lower than measured at Kevo

Supporting Information:
- Figures S1–S7

Correspondence to:
L. Husain,
lhusain@albany.edu

Citation:
Dutkiewicz, V. A., A. M. DeJulio, T. Ahmed, J. Laing, P. K. Hopke, R. B. Skeie, Y. Viisanen, J. Paatero, and L. Husain (2014), Forty-seven years of weekly atmospheric black carbon measurements in the Finnish Arctic: Decrease in black carbon with declining emissions, *J. Geophys. Res. Atmos.*, *119*, 7667–7683, doi:10.1002/2014JD021790.

Received 20 MAR 2014
Accepted 23 MAY 2014
Accepted article online 16 JUN 2014
Published online 18 JUN 2014

Forty-seven years of weekly atmospheric black carbon measurements in the Finnish Arctic: Decrease in black carbon with declining emissions

Vincent A. Dutkiewicz[1,2,3], Anthony M. DeJulio[2], Tanveer Ahmed[3], James Laing[4], Philip K. Hopke[4], Ragnhild B. Skeie[5], Yrjö Viisanen[6], Jussi Paatero[6], and Liaquat Husain[1,2,3]

[1]Atmospheric Sciences Research Center, State University of New York, Albany, NY, USA, [2]Department of Environmental Health Sciences, School of Public Health, State University of New York, Albany, New York, USA, [3]Wadsworth Center, New York State Department of Health, Albany, New York, USA, [4]Center for Air Resources Engineering and Science, Clarkson University, Potsdam, New York, USA, [5]Center for International Climate and Environmental Research, Oslo, Norway, [6]Finnish Meteorological Institute, Observation Services, Helsinki, Finland

Abstract Concentrations of atmospheric black carbon, [BC], were determined from filter samples collected weekly at Kevo, Finland (69°45′N, 27°02′E), from 1964 to 2010 using optical and thermal optical methods. The data provide the longest record of *directly* measured [BC] in the Arctic. The mean winter, spring, summer, and autumn [BC] based on the entire data set were 339, 199, 127, and 213 ng m^{-3}, respectively. Annual mean [BC] decreased from ~300 in ~1970 to 82 ng m^{-3} in 2010. [BC] data sets from other Arctic sites show similar trends, but concentrations at Kevo are generally higher. From ~1970 to 2010 the [BC] decreased by ~1.8% yr^{-1}. However, [BC] did not decrease monotonically. Instead, cyclical peaks occurred around 1976–1977, 1985–1987, and 1999. During such periods, nickel concentrations were well correlated with [BC]. This suggests that emissions from extensive ore smelting on the Kola Peninsula were significant contributors of particulate matter observed at Kevo. Simulations of [BC] at Kevo using the OsloCTM3 model using different emission inventories and meteorological data sets were performed. Modeled concentrations were lower than observed by a factor of 4. The results indicated that circulation changes can explain year to year variability, but the downward trend in the observations is mostly explained by emissions. Emission inventories in Europe, Russia, and the former Soviet Union are poorly constrained and appear to need revision in order to match observed trends in BC atmospheric concentrations.

1. Introduction

Elemental or black carbon particles in the atmosphere are of considerable importance because of their impact on visibility, climate forcing [*Novakov et al*., 2003; *Jacobson*, 2002; *Ramanathan and Carmichael*, 2008; *McConnell et al*., 2007; *Bond et al*., 2013], and adverse health effects [e.g., *Dockery et al*., 1993; *Pope et al*., 2002; *Forastiere*, 2004; *Rom and Samet*, 2006]. The terms elemental carbon (EC) or black carbon (BC) are often used interchangeably, but they really reflect the difference in measurement method [*Salako et al*., 2012]. BC is a primary pollutant emitted as a by-product of incomplete combustion of fossil fuel, biomass, and biofuel. BC particles are submicron in size; ~95% have aerodynamic diameter < 2.5 μm [*Viidanoja et al*., 2002; *Begum et al*., 2011]. BC particles strongly absorb solar radiation and impact the Earth's temperature. In fact, BC may be the second largest contributor to global warming after greenhouses gases. However, the magnitude of the climate forcing by BC is quite uncertain, with a global average value estimated up to +1.1 W m^{-2} [*Bond et al*., 2013].

Wet deposition is the main route for removal of BC from the atmosphere [*Ogren and Charlson*, 1983]. The mean residence time of particulate BC in the lower troposphere has been estimated at about 6 days [*Haywood and Shine*, 1995]. As a result, BC particles can be transported over thousands of kilometers before being removed from the atmosphere. During the winter, the polar front moves south to encompass the BC emission source areas in Europe and Eurasia. The cold air north of the front provides stable atmospheric conditions and lack of removal processes, enhancing the long-range transport [*Iversen and Joranger*, 1985;

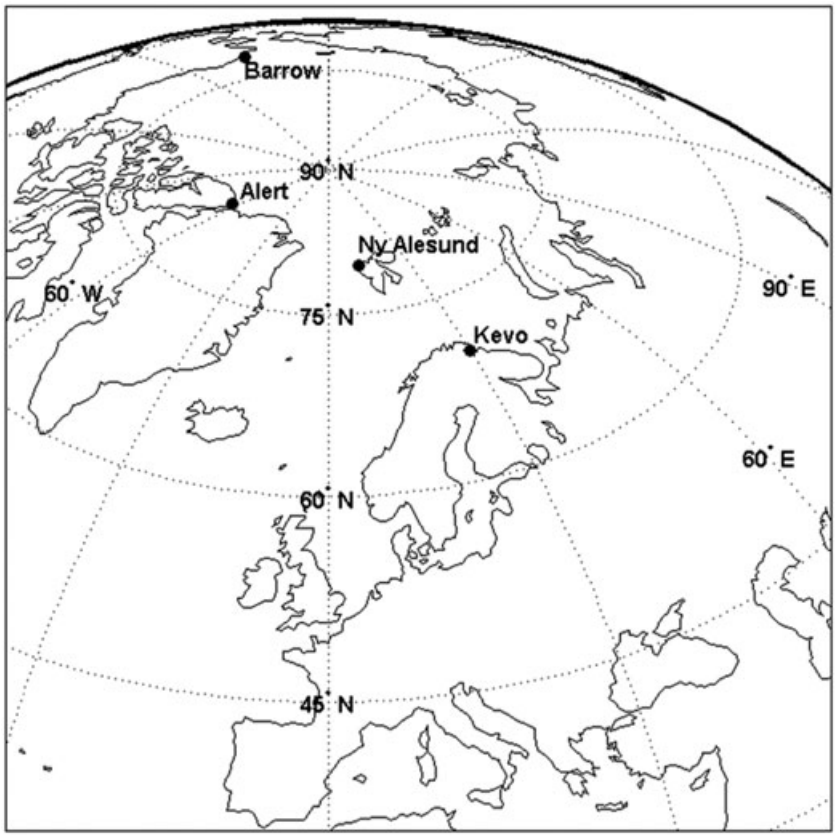

Figure 1. A map showing the location of the sampling site at Kevo (69°45′N, 27°02′E) and three additional Arctic sampling sites referenced in the text; Alert (82.5°N, 62.5°W), Barrow (72.0°N, 156.3°W), and Ny Ålesund (78.9°N, 11.9°E). The Kola Peninsula is the projection of land just southeast of Kevo.

Raatz and Shaw, 1984; *Shaw*, 1995]. Therefore, [BC], at a given location is highly dependent upon the distance from emission sources and scavenging losses along the transport route.

There are few BC sources in the Arctic. Large amounts of fossil fuels used in the US, Canada, Europe, and the Soviet Union have significantly contributed to BC in the Arctic air [e.g., *Polissar et al*., 2001; *Sharma et al*., 2004]. Deposition of BC on Arctic snow and ice allows absorption of solar radiation and causes it to melt more readily [*Warren and Wiscombe*, 1980; *Hansen and Nazarenko*, 2004; *Flanner et al*., 2009]. Direct long-term atmospheric measurements in the Arctic are required to evaluate the regional BC contributions and to develop a strategy to minimize its impact on climate. Additional measurements of trace elements, major ions, methane sulfonic acid, and air trajectories have been made to characterize aerosol composition at the site and evaluate source regions [*Laing et al*., 2013, 2014a, 2014b]. In this paper we (1) report the measurements of [BC] on filters collected over 47 years at Kevo, Finland, (2) study the seasonal and long-term trends in [BC], (3) evaluate the relative impact of potential source regions, and (4) compare the measured [BC] with the values calculated by a model that simulates BC transport and removal rates and uses emission inventories as input.

2. Experimental Methods

2.1. Sample Collection at Kevo, Finland

The sampling station at Kevo (Figure 1) is located 350 km north of the Arctic Circle at an altitude of 98 m [*Paatero et al*., 1994a]. It is near Lake Kevojärvi close to the Kevo Nature Reserve, a protected area of 712 km^2. The site is situated in the birch subzone of a boreal coniferous forest. The area is sparsely populated (0.4 inhabitant km^{-2}). Mean temperature of the coldest month (January) is −14°C and the warmest month (July), +13.1°C. The annual mean temperature is −1.3°C. The ground is usually covered by snow from October until

mid-May. The mean annual precipitation is about 43.3 cm of which 30–40% falls as snow [*Yli-Tuomi et al*., 2003; *Pirinen et al*., 2012].

Total suspended particles were collected on one of two filter holders that ran alternately for 4 h intervals from 1964 thru 2010 [*Paatero et al*., 1994b]. From 1964 to 1978, the two units were equipped with rectangular 12 cm × 14 cm Whatman 42 (W42) filters. The W42 filters were supported with a fine grid and collected particles uniformly over the exposed area (11 cm × 13 cm, 286 cm^2). The mean total air volume was ~1200 m^3. We received ¼ of each of the filters. The W42 filter collection ended in March 1978. No samples were collected until January 1979 while the sampling system was modified.

Since January 1979 glass fiber (GF) filters have been used with a modified collection system. Two alternately running collectors were still used, but the GF filters were wrapped around a cylindrical body that had a 9 mm square grid [*Paatero et al*., 1994a, 1994b]. The grid did not allow a uniform collection of particles over the entire filter. Instead, each filter consisted of a series of 9 mm squares with particles separated by a 2 mm strip with no particles. The exposed area was reduced to 194 cm^2, and the total air volume varied from 3000 to ~5500 m^3.

2.2. Determination of BC Concentrations in Individual Weekly Filters

In all, there were 2280 weeks sampled or 4560 filters were collected over the 47 years. Currently, the most widely accepted technique used to measure [BC] is the thermal/optical method with either transmission or reflectance pyrolysis correction (designated as TOT or TOR, respectively). The most commonly applied protocols, using different temperature regime for the extraction of organic carbon or BC, are the TOT National Institute for Occupational Safety and Health (NIOSH) method [*Birch and Cary*, 1996] and the TOR Interagency Monitoring of Protected Visual Environments (IMPROVE) method [*Chow* et al., 1993]. A comparison of the methods reported that total carbon measured by the TOT and the TOR protocols were statistically equivalent but that the TOT protocol yielded consistently higher BC than the TOR protocol by around a factor of 2 [*Chow et al*., 2001]. As there is no generally accepted standard for BC, neither method can claim to be more reliable. The TOT NIOSH protocol was used in this study.

2.2.1. Whatman 42 Filters

The standard thermal optical methods require that the aerosols to be on a quartz filter, so BC cannot be directly determined on W42 filters. We earlier developed a technique that used $ZnCl_2$ to dissolve the cellulose, so the aerosols can be transferred onto a quartz filter and [BC] measured by the TOT method [*Li et al*., 2002]. Using spiked standards that varied from 1.31 to 5.06 mg, *Li et al*. [2002] established that recoveries varied from 87 to 99% with a mean of 93%. The method, however, is time consuming and costly when thousands of samples have to be analyzed. Therefore, for this study all W42 filter samples were analyzed by a relatively faster optical method using a commercial Optical Transmissometer, OT21 (Magee Scientific Corporation). In addition, we analyzed 72 samples collected in January and July using the TOT NIOSH method. Therefore, we had a robust comparison of the optical method with the thermal optical method, allowing us to validate the optical method against the most widely used method. Table 1 summarizes the filter collection and methods used to determine [BC].

2.2.2. Glass Fiber Filters

Unlike W42 filters, GF filters can be directly used for the measurement of [BC] either by the optical or thermal optical method. As for the W42 filters, we decided to analyze all GF filters using the faster optical methods but validate the method by analyzing weekly samples from January and July for 13 years along with two additional full years by the thermal optical method as outlined in Table 1.

2.3. Determination of [BC] by the Thermal Optical Method

2.3.1. Whatman 42 Filters

[BC] for the W42 filters were determined using the same methodology that we have used for many years for Whatman 41 filters [*Li et al*., 2002; *Husain et al*., 2008; *Khan et al*., 2006]. Two 25 mm diameter discs were punched from each W42 filter samples, dissolved in 70% $ZnCl_2$ solution at 70°C, and the BC was transferred on to quartz filters using the method given in *Li et al*. [2002]. After the filter was dried under vacuum, [BC] was determined individually for three aliquots of each sample with a Sunset Laboratories TOT carbon analyzer following the NIOSH 5040 protocol [*National Institute for Occupational Safety and Health* (*NIOSH*), 1996]. Uncertainties were based on the instrument error output by the Sunset protocol. The detection limit of [BC] was 0.2 $\mu g\, cm^{-2}$ which corresponds to a [BC] of 10 $ng\, m^{-3}$ at a volume of 1500 m^3.

Table 1. Description of Filter Collection Types and Analytical Methods Used for [BC] Determinations

					TOT BC Determination	
Filter Type	Filter Characteristics	Volume (m^3)	In Use Dates	Optical BC Determination	Time Periods	Method
Whatman 42, two per week	homogeneous deposition 12 × 14 cm filter, exposed area = 286 cm^2	~1200	October 1964 to March 1978	all weekly filters (n = 1346)	January and July (1965–1968 and 1970–1978, n = 72)	$ZnCl_2$ digestion with filtration onto quartz filter followed by NIOSH TOT analysis[a]
Glass Fiber, two per week	9 mm grids with 2 mm strip between each grid, exposed area = 196 cm^2	3000–5500	1979–2010	all weekly filters (n = 3278)	January and July (1979–1981, 1986–1988, 1993–1995, 2000–2002, and 2008–2010) plus all samples for 1988 and 1993 (total n = 176)	BC directly determined on GF filter using modified temperature protocol[b]

[a] *Li et al.* [2002], section 2.3.1.
[b] Protocol provided by Sunset Laboratories, section 2.3.2.

2.3.2. Glass Fiber Filters

The BC measurements of the GF filters were straightforward compared to the method for the W42 as the Sunset analyzer has a built-in protocol specifically to measure [BC] on GF filters. A 1 × 1.5 cm prebaked quartz filter punch is placed in the oven boat, and a 1 cm square punch is taken from the GF filter and placed centered on top of the quartz base. The GF protocol uses modified temperature and dwell times to measure BC. The manufacturer has indicated (B. Cary, personal communication, 2014) that if there is excessive organic carbon from fresh biogenic burning, this protocol may over estimate [BC] but if the sources are predominantly vehicular or diesel, the error would be small. With the changeover of heating from wood to electricity at the facility in 1970 local wood burning is not a factor at the site in 1979 when sampling was switched to GF filters. BC determinations were made for two squares on each filter or on four squares for each weekly sample collected in January and July for selected years and for two complete years as outlined in Table 1. Uncertainties were computed based on instrument errors output by the Sunset protocol.

2.4. Measurements of [BC] Using the Optical Transmissometer, OT21

The Beer-Lambert law is the basis for the determination of BC in aerosols for optical techniques. The method assumes that BC is the only component in particulate matter that is light absorbing. The amount of light absorbed is proportional to [BC] and can be expressed by $[BC] = 100 \times \ln(I_o/I)\,[\sigma_a(\lambda)]^{-1}$ [A/V], where I_0 and I are the intensity of the light passing through a blank filter and a filter containing aerosols, respectively, $\sigma_a(\lambda)$ is the absorption/attenuation coefficient (in $m^2\,g^{-1}$) for a light source with a wave length λ, A is the area of the filter, and V is the volume of the air sampled through the filter.

Incident light with wavelength of 880 nm is most frequently used for BC measurements, as was the case in this work. The standard $\sigma_a(\lambda)$, 16.6 $m^2\,g^{-1}$, suggested by the manufacture was used. The transmission intensities, I_0 and I were measured through a blank and an aerosol-loaded filter, respectively. It is important that the blanks used reflect the time period being analyzed as aging may affect the optical properties of some filter media. We have used edges of actual samples and samples which were not run to verify the blank values used in this study. We describe below the methodology used in this work for W42 and GF filters.

2.4.1. Whatman 42 Filter Analysis

A pair of 25 mm diameter discs was cut from each of the two filters, and the transmission intensities determined by the OT21. Each [BC] is based on the mean of four determinations. Uncertainty was evaluated as a function of absorption by measuring BC from multiple pairs of filter measurements and variability of filter blanks as discussed elsewhere [*Ahmed et al.*, 2009].

2.4.2. Glass Fiber Filters

As indicated earlier, the particle collection on the GF filters was different from that for W42. Each GF filter consisted of a series of 9 mm squares with particles separated by a 2 mm strip with no particles. Thus, the GF filters could not be directly placed in the OT21 for measurement. Unlike its optical cousin, the aethalometer, Magee indicates that the OT21 requires a homogeneous deposition of particulate matter over the 15 cm diameter analytical zone for proper operation. The reason for this is that the aethalometer uses the difference in transmission between times t_1 and t_2 to evaluate BC, while the OT21 uses a single-transmission measurement through a defined area relative to a blank to measure the BC optical density. To circumvent the problem, we prepared a pair of 8.9 mm masks made out of a heavy gauge aluminum foil. One mask was placed on the blank reference filter, and the second mask was placed over the sample, so the light could only pass through the filter area where particles were deposited. An aliquot with four deposited areas was cut from each of the two filters collected during each sampling cycle, so eight grid areas were analyzed and averaged for BC determination in each weekly sample. To evaluate the precision of this method, the standard deviation of first 50 filters analyzed were evaluated. The BC density varied from 0.1 to 15 $\mu g\,m^{-2}$. The filters with BC density $> 2\ \mu g\,m^{-2}$ had a relative standard deviation between the four determinations that averaged 6%. This confirms that good precision was obtained with the optical method.

2.4.3. Shadowing Correction for Optical BC Determinations

For optical [BC] determinations, scattering in the upper layers of aerosols can diminish the absorption of the light beam by underlying aerosols causing an underestimation of [BC] [*Liousse et al*., 1993; *Petzold et al*., 1997]. This is especially important when particle loading is high. While the specific attenuation coefficient (σ) recommended by the manufacturer was empirically determined and, in part, accounts for this effect at low to moderate loading levels, samples with high aerosol loading certainly require correction [e.g., *Park et al*., 2010]. Several approaches for shadowing corrections have been suggested [*Weingartner et al*., 2003; *Schmid et al*., 2006; *Virkkula et al*., 2007]. We chose to use the formulation suggested by *Virkkula et al*. [2007] that was further validated by *Park et al*. [2010]:

$$[BC]_c = [BC]_{uc}\{1 + k \times \mathrm{ATN}\} \quad (1)$$

where $\mathrm{ATN} = (100 \times \ln(I_o/I))$, $[BC]_{uc}$ denotes the direct measurement by the OT21, k is the shadowing correction, and $[BC]_c$ is the final [BC] corrected measurement. Comparison between the OT21 and TOT results is used to establish appropriate k values for each filter type, as discussed below.

3. Results

3.1. Comparison of [BC] Measurements by the Optical and Thermal Optical Methods

3.1.1. Measurements in Whatman 42 Filters

Concentrations of BC were determined, both by optical and thermal optical methods as described above, in 72 W42 weekly samples collected from 1965 to 1968, and 1970 to 1978 (Table 1). The data are plotted in Figure 2a along with uncertainties in the optical measurements. Uncertainties varied from around 75% at $[BC] = 50\ ng\,m^{-3}$, 50% at $[BC] = 100\ ng\,m^{-3}$, and 25% at $[BC] = 400\ ng\,m^{-3}$, to 16 to 20% for $[BC] > 600\ ng\,m^{-3}$. The linear regression shows a very good correlation ($r^2 = 0.91$) between the two techniques, but the slope is only 0.36 (Figure 2a). Removing the very high point at $\sim 1600\ ng\,m^{-3}$ does not significantly alter the slope, but r^2 is decreased to 0.85. The data show that the [BC] values tend to deviate from linearity above $[BC] \sim 500\ ng\,m^{-3}$. We suggest that this is due to the shadowing effect, as it has been observed by others [*Liousse et al*., 1993; *Petzold et al*., 1997]. We used equation (1) and varied k for the OT21 data to give the best linear regression passing through the origin and a slope of ~1.0. The result with $k = 0.025$ is shown in Figure 2b. Note that the slope is 1.0 and r^2 is 0.92. *Virkkula et al*. [2007] reported k values for aethalometer measurements at sites in Finland that varied between 0 and 0.015 with a mean of 0.0018. The k value for W42 is somewhat above this upper range, but we are not aware of any other measurements of [BC] using this substrate. However, Figure 2b demonstrates that optical BC measurements can yield reliable BC results once appropriate shadowing corrections are applied.

During 1965 and 1966 the median ATN in W42 filters was around 21. Hence, the correction due to shadowing would be large, >53%. However, as we show later the data for these years and through 1970 are not further considered in the paper. For samples from 1971 to 1977 the median ATN was < 16, and hence, annual shadowing corrections were on the order of 20%.

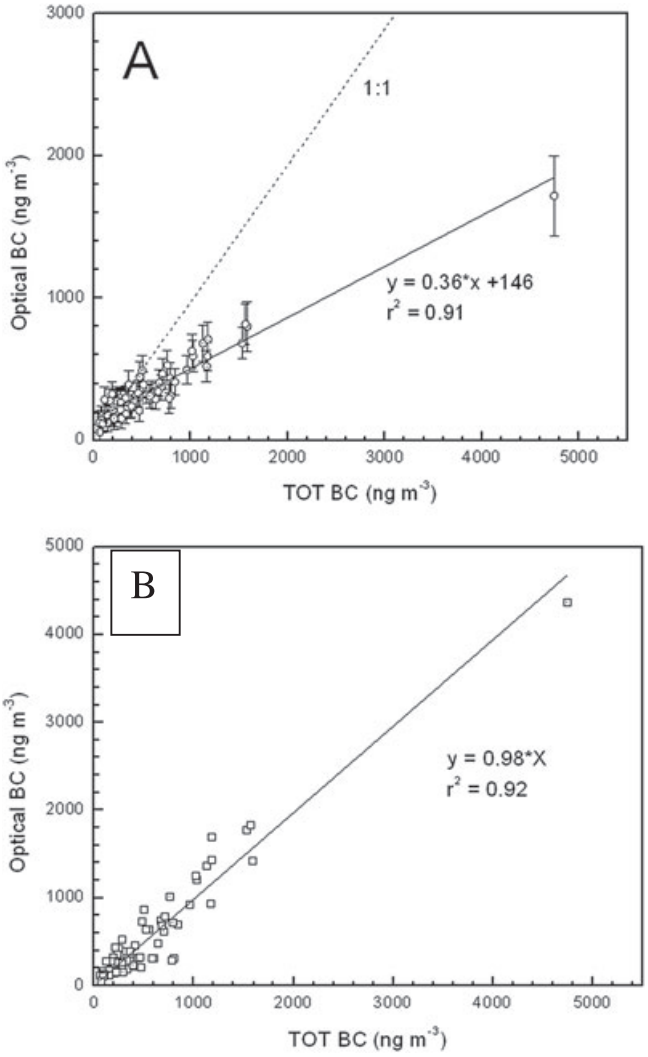

Figure 2. (a) Scatterplot comparing [BC] measured in weekly W42 samples at Kevo by optical and the thermal optical methods. (b) Data have been corrected using equation (1), and $k = 0.025$. The solid lines in both panels are linear regression with the regression in B forced to pass through the origin.

3.1.2. Measurements on Glass Fiber Filters

All weekly samples collected on GF filters in 1988 and 1993,and weekly samples collected during each January and July of 1979–1981, 1986–1988, 1993–1995, 2000–2002, and 2008–2010 (in all 176) were analyzed by both thermal optical and optical methods. The data are shown in Figure 3a along with uncertainties. In general, uncertainties for the BC measurements on the GF filters are lower than those for W42. For example, the average uncertainty at [BC] = 50 ng m^{-3} is 30%, at [BC] = 100 ng m^{-3} the uncertainty is 20%, and [BC] $>$ 300 ng m^{-3} has an average uncertainty of 14%. As was the case for W42 filters, an increasing deviation from linearity is observed with higher concentrations. A linear regression forced through the origin has a very good r^2, 0.92, but the slope is 0.76, indicating a slight underestimation of [BC] by OT21 at higher loadings. Accounting for shadowing correction thru the use of equation (1) yields a slope of 1.0 and $r^2 = 0.96$ with a value of $k = 0.0021$ (Figure 3b). To evaluate the uncertainty in k, we varied k, so the regression slope varied between 0.95 and 1.05 and found the variation on k of only ±0.0005, suggesting that k is well defined for the GF filters. The k required for GF filters is a little more than a factor of 10 lower than the k required for the W42 filters, and it is actually quite comparable to the k values commonly used to correct aethalometer data [*Virkkula et al*., 2007; *Park et al*., 2010]. Thus, the two techniques yielded results in excellent agreement with each other, and corrected OT21 values can accurately determine BC in GF filters.

The median ATN for GF filters collected in 1979–1988 was around 72, much higher on average than those for the W42 measurements. However, because k for GF filters is around a factor of 10 lower than that for W42, the net impact on quarterly and annual means for the GF filters were still relatively small (~17%). Moreover after 1988, [BC] decreased sharply with median ATN varying between 18 and 32, thereby further reducing the impact of the shadowing correction.

3.2. Weekly and Seasonal Variations

Yli-Tuomi et al. [2003] used sections of the same W42 filters collected at Kevo to measure trace elements by neutron activation, sulfate, and major ions by ion chromatography, and BC by optical transmission. BC was measured on an early prototype of the OT21 using results for the 880 nm channel and no shadowing corrections. The *Yli-Tuomi et al*. [2003] BC values were higher than our uncorrected results by around 20%. As BC is inversely proportional to $\sigma_a(\lambda)$ and *Yli-Tuomi et al*. [2003] used $\sigma_a(\lambda)$ of 15.0 compared to the value of 16.6

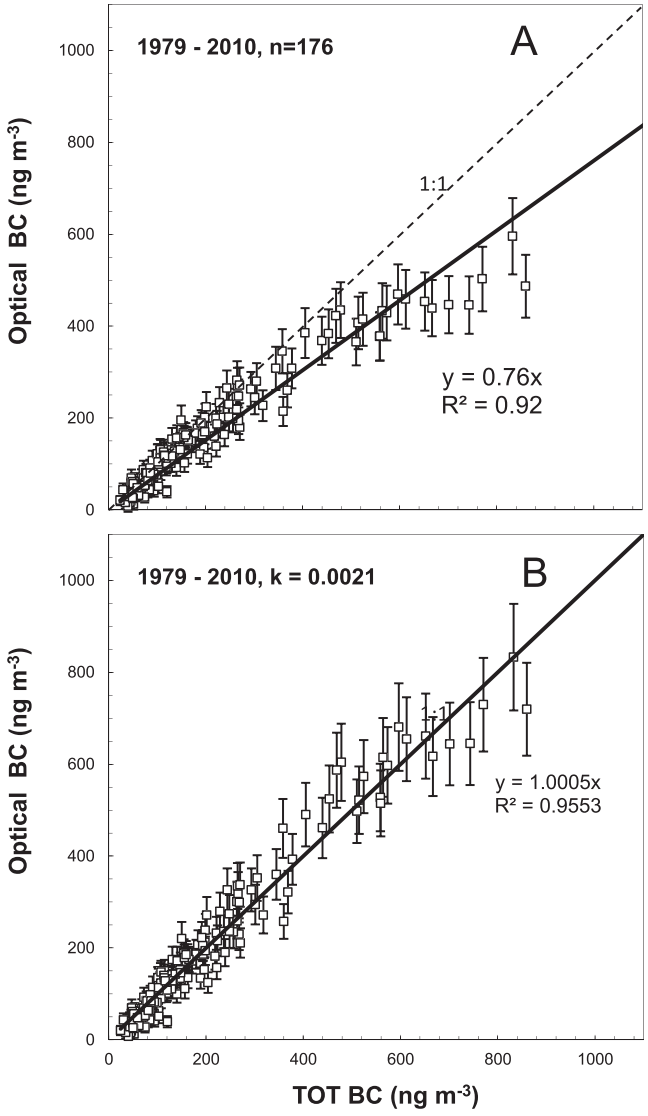

Figure 3. Scatterplots comparing [BC] measurements by OT21 and the thermal optical method in weekly samples collected on GF filters as defined in Table 1. (a) Raw data are shown, and the solid line is a linear regression forced through the origin while the dashed line is the 1:1 reference line. (b) The OT21 data have been corrected for shadowing using equation (1), and $k = 0.0021$. The solid line is a linear regression passing through the origin.

used here, their results are expected to be at least 11% higher. Annual means for 1965–1977 normalized to 1965 differ by 1 to 24% with a mean of 11%. This demonstrates that there is very good agreement between the BC trends for the two sets of measurements.

Weekly [BC] at Kevo for the entire period are shown in Figure 4. There were only 11 weekly measurements available in 1964, and these are not shown. The data show that weekly [BC] exceeded 1000 ng m^{-3} with decreasing frequency over time (20 events 1965–1969, 17 events 1970–1979, 6 events 1980–1989, and none during 1990–2010). Wood was burned at the site during winter months for heating until the end of 1970, so the high [BC] values observed during this period may have some contribution from this source. For an estimation of the global warming from BC, it is the regional BC values which are needed. Hence, we have flagged the data for this period and will not include these years in consideration of long-term trends. The [BC] quarterly means for each year are shown as dark horizontal lines (Figure 4), and 5 year quarterly mean [BC] beginning in 1971 are given in Table 2. Generally, the highest [BC] was observed during the first quarter. The Sun does not shine at Kevo from late November through mid-January, so the site is within the Arctic vortex and experiences stagnation and enhanced pollutant lifetimes [*Shaw*, 1995]. During the first quarter (January through March), the [BC] varied from 491 in 1971–1975 to 164 ng m^{-3} in 2006 to 2010, with a mean value of 323 ng m^{-3}. Similarly, the ranges and the means for the second, third, and fourth quarters were 382 to 86 with a mean of 168, 195 to 61 with a mean of 120, and 270 to 80 with a mean of 187 ng m^{-3}, respectively. Thus, the highest concentrations were observed during the first quarter and lowest during the third. Mean BC contributions during the various quarters were 41, 21, 15, and 23% for the first, second, third, and fourth quarters, respectively. This pattern is consistent with the seasonal pattern reported for other Arctic sites [*Sharma et al.*, 2013]. The data in Table 2 demonstrate that [BC] has significantly decreased over all seasons. The decline in [BC] at the site can be examined more accurately by examining annual concentrations below.

3.3. Long-Term Trends in [BC] and Comparison With Other Arctic Sites

The most striking feature of the BC trend is that the concentrations, whether weekly or seasonal means, exhibited a remarkable decrease with time (Figure 4). We used the data to compute annual mean [BC] and

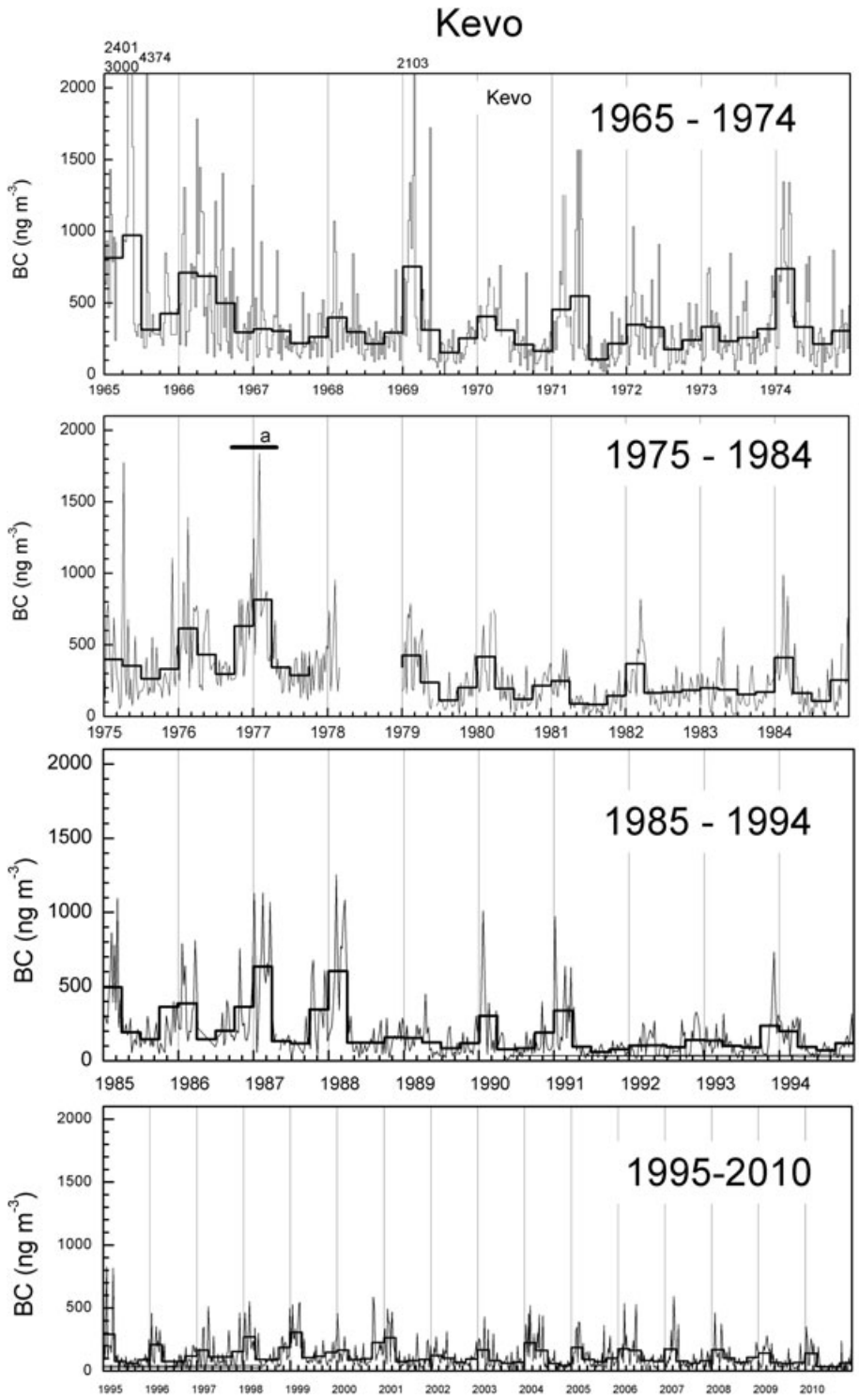

Figure 4. The [BC] determined in weekly samples collected at Kevo from 1965 to 2010. The dark horizontal lines are quarterly means.

plotted the results in Figure 5. The annual [BC] values for 1965 and 1966 were, respectively, 634 and 548 ng m^{-3}. Following the high [BC] observed in 1965–1966, concentrations decreased to 276 ng m^{-3} in 1967 and the annual concentrations through 1970 period were similar to those for the 1971 thru 1973, a period of 3 years after the wood burning ceased. Thus, the data do not support a large wood burning

Table 2. Mean Quarterly Concentrations of BC (ng m^{-3}) for 5 Year Periods From 1971 to 2010

	1971–1975	1976–1980	1981–1985	1986–1990	1991–1995	1996–2000	2001–2005	2006–2010
January–March	491	539	351	422	203	216	198	164
April–June	382	304	162	113	95	92	107	86
July–August	195	205	133	124	73	96	70	61
September–December	290	348	190	207	141	158	84	80

contribution, at least, not for 1967 thru 1970. Still, we have included the annual mean [BC] for the 1965 to 1970 years in Figure 5 but have not included these data in calculating the long-term decrease in [BC].

[BC] has decreased very significantly since 1971. However, the decline was not monotonic. [BC] values were fairly constant from 1967 thru 1973, but then they increased to a peak value of 500 ng m^{-3} in 1976. Another peak in [BC] was observed around 1986 through 1988, although lower in concentration, ~300 ng m^{-3}. We will discuss the sources of these elevated concentrations in section 4.1. Subsequently, [BC] has slowly decreased with the exception of somewhat elevated concentrations in 1998–2000 with values in the range 144–168 ng m^{-3}. In 2010 [BC] averaged only 67 ng m^{-3}. Taking the average [BC] around 1971 to be 300 ng m^{-3}, there has been a 78% decrease over 40 years or an effective decrease rate of 1.8% yr^{-1}. The seasonal Mann-Kendall trend test associated with Sen's slope result yields a statistically significant ($p < 0.001$) decreasing trend of 1.9% yr^{-1}. Clearly, there is a significant decreasing trend for [BC] at Kevo.

The two other long running [BC] measurement campaigns in the Arctic are at Barrow, Alaska [*Bodhaine*, 1989; *Polissar et al*., 1999], and Alert, Canada [*Sharma et al*., 2004, 2013; *Gong et al*., 2010]. The latter is closest to Kevo. At Alert [BC] was determined for 1989 through 2007 using an aethalometer cross calibrated to a two-step thermal method. Thus, they used an effective attenuation coefficient of 19 m^2 g^{-1} and applied no loading corrections. Their data are shown in Figure 5. On average Alert [BC] values are 50% lower than at Kevo. Based solely on the higher attenuation coefficient used at Alert, [BC] would be expected to be 14% lower than at Kevo. The sites, however, are well separated with Kevo located much closer to major BC source regions. At Alert [BC] decreased from 90 ng m^{-3}in 1989 to 35 ng m^{-3} in 2007, a 61% decrease over 18 years or a decrease of 3.4% yr^{-1}. The nonparametric Sen Analysis by *Gong et al*. [2010] yielded 2.3%–3.4% decrease per year for January to April. *Sharma et al*. [2004] attributed the decrease in [BC] at Alert to the collapse of the economy in the USSR, and they presented emission calculations to support their suggestion. We discuss this hypothesis further in section 4.3.

We also show in Figure 5 measurements of annual [BC] from 1991 to 2004 from the Zeppelin station, Ny Ålesund, Svalbard, Norway made using the optical method on W41 filters [*Husain et al*., 2011]. Also shown are annual means based on aethalometer [BC] measurements at this site for 1991, and 2001–2007 by *Eleftheriadis*

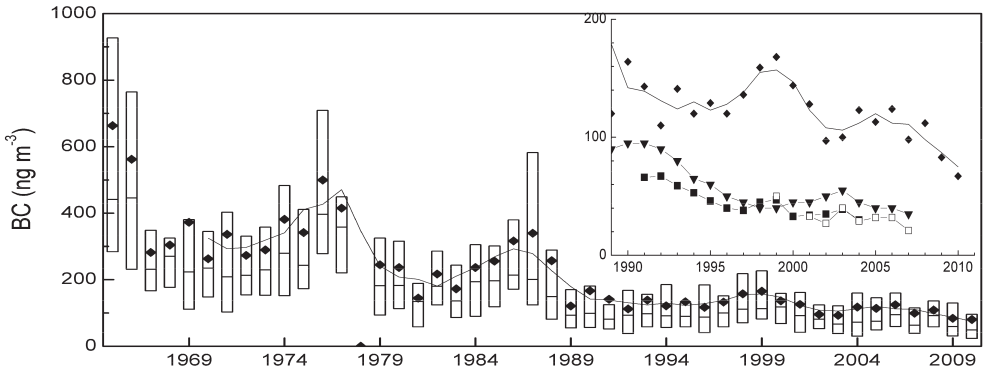

Figure 5. Annual mean [BC] at Kevo for 1965–2010. Bars show 25th and 75th percentile ranges; horizontal lines are medians and diamonds are means. Trend line is 3 years running mean starting in 1970 as earlier data may have local wood burning component. Insert shows 1989 until 2010 on an expanded scale with data from Alert, Canada (solid triangles, from Figure 1b [*Gong et al*., 2010]), and Ny Ålesund (Svalbard, Norway). Solid squares are from *Husain et al*. [2011], while the open squares are from *Eleftheriadis et al*. [2009].

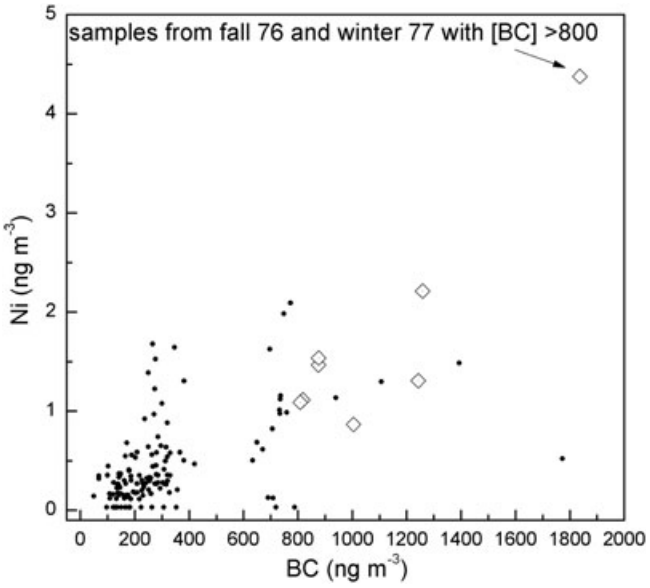

Figure 6. Scatterplot of water-extracted Ni [*Laing et al*., 2014a] versus BC concentrations for Kevo samples collected in fall 1976 and winter 1977. Diamonds highlight samples from October 1976 to March 1977 with BC concentration > 800 ng m^{-3}.

et al. [2009]. The two sets of measurements at Ny Ålesund agree very well where they overlap and they are a little lower than the concentrations observed at Alert. For the combined 17 years of [BC] measurements at Ny Ålesund, there is a 56% decrease in [BC] or a declining rate equivalent to 3.3% yr^{-1}, compared to ~1% yr^{-1} trend for the same period at Kevo. While all three Arctic sites demonstrate a decreasing [BC] trend after 1990, the trends are smoother at Alert and Ny Ålesund compared to that at Kevo. In particular, the increased [BC] during 1996–2000 at Kevo is not seen at other sites. Clearly, the proximity of Kevo to emissions in Europe and Russia is a major factor. Once we are confident with emission inventories so models can simulate [BC] at Kevo, these models can then be used with added confidence to assess the impact of these emissions on the high Arctic.

4. Discussion

4.1. Source(s) of Elevated [BC] in ~1976

It was noted earlier that the annual mean [BC] values in 1976 and 1977 were elevated. There were unusually high [BC] during the fall of 1976 and the winter of 1977 as there were 9 weeks (designated as **a** in Figure 4) when [BC] exceeded 800 ng m^{-3}. Soluble and total digested trace element concentrations were also measured for these samples [*Laing et al*., 2014a]. Of about 40 elements measured, only Ni had elevated concentrations concurrently with high [BC] during this period. A scatterplot of weekly water-extracted [Ni] versus [BC] between 1975 and 1977 is shown in Figure 6. There is clearly a strong association between the two species as high concentrations generally occur at the same time (correlation coefficient = 0.68). Of the nine weekly samples collected between October 1976 and March 1977 with [BC] > 800 ng m^{-3}, Ni concentrations are available for eight samples shown as diamonds in Figure 6. The highest BC and Ni occurred on 24 January to 31 January 1977 (BC = 1835 ng m^{-3} and Ni = 4.4 ng m^{-3}). *Yli-Tuomi et al*. [2003] pointed out that emissions from smelting and industrialization on the Kola Peninsula strongly impact Kevo. The majority of emissions on the Kola Peninsula come from nonferrous ore roasting and metal smelting facilities [*Tuovinen et al*., 1993]. Estimates of Ni, Cu, and Co emissions on the peninsula for 1994 were 1916, 1097, and 92.1 t/yr, respectively [*Boyd et al*., 2009]. Additional discussion of heavy metal emissions in this region are given in *Laing et al*. [2014a]. Hybrid Single-Particle Lagrangian Integrated Trajectory (HYSPLIT)4 backward in time air trajectories [*Draxler and Hess*, 1998] with the REANALYSIS meteorological data set and a 500 m starting height were run for all samples. Figure S1 in the supporting information shows the HYSPLIT4 plot for the 3 day back trajectories originating daily (noon local time) over 24–31 January 1977. With the exception of the 30 and 31 January trajectories, all five other trajectories pass through the Kola Peninsula. In addition, all of these trajectories, except 30 January, are linked with near-surface air making it very likely that they were enriched with pollutants on the Kola Peninsula. The high Ni concentrations, coincident with high [BC], suggest that they also are impacted by emissions from the Kola Peninsula. The fact that the BC is associated but not highly correlated with Ni suggests that their sources are in the same region, though not necessarily the same source. The trajectories also passed over Murmansk, Russia, which is a large active port city and was more likely to be the source of the high [BC].

We further explored the influence of emissions from Kola Peninsula by examining the relationship between Ni and [BC] for the entire period. In Figure 7, we have shown the annual mean [BC] along with the [Ni]. The

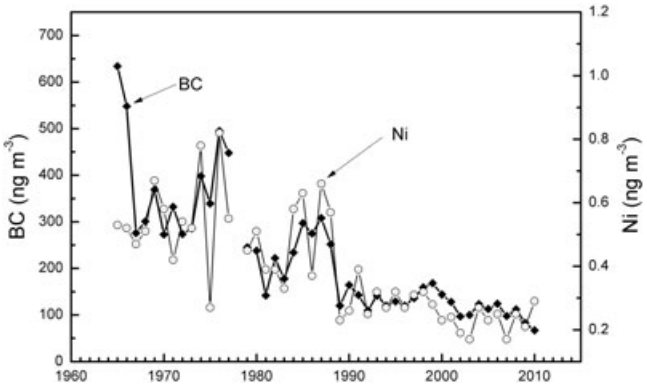

Figure 7. Time series plots of annual mean [BC] and [Ni] [*Laing et al.*, 2014a] measured at Kevo, Finland.

variations in their concentration is remarkably similar for the entire period (correlation coefficient, *r*, over 1967–2010 annual means is 0.86). Note that the periods with elevated [BC] in 1976 and 1977 and 1985–1987 correspond to periods with elevated Ni concentrations. An inescapable conclusion is that, indeed, the Kola Peninsula emissions contributed very significantly to the [BC] observed at Kevo at all times during the observation period. This suggestion finds further support in an assessment of emission source contribution using Potential source contribution function (PSCF) described below in section 4.2.

4.2. Evaluation of [BC] Source Regions by PSCF Analysis

Potential source contribution function is a way of assessing source contribution regions for large data sets using backward in time air trajectories [e.g., *Cheng et al.*, 1993; *Fan et al.*, 1994; *Polissar et al.*, 1999, 2001]. Specifics of the application of the method to the Kevo trace metal data set are presented by *Laing et al.* [2014b], so only salient features are given here. For this analysis 5 day back trajectories were computed twice daily over the whole analysis field using HYSPLIT4. Thus, 14 trajectories were computed for each sample. The geographical region of interest is divided into 2.5 km × 2.5 km grid cells [*Fan et al.*, 1994]. It is assumed that if a trajectory passes through a grid cell, a component proportional to the source strength is transported to the receptor site. The ratio of the number of trajectory end points associated with high concentrations to the total number of trajectory end points passing through a grid cell gives the probability that this grid cell is a source of high concentrations of the specie of interest at the receptor. For this analysis the high-concentration cutoff was taken as > the mean. Further details can be found in *Laing et al.* [2014b]. Usually, local sources cannot be clearly identified using PSCF.

PSCF maps were generated for 1964–1990 and 1991–2010 separately for each of the four seasons. The maps for winter, spring, and summer for both periods are shown in the supporting information (Figures S2–S7); the spring and fall maps were similar. The map for summer 1991–2010 (Figure S2) does not have any well-defined source regions. The highest probability regions are only 0.4–0.6, and they cover essentially all of Europe and Russia. Winter is the most important season with regard to BC deposition in the Arctic, as ~40% of the annual [BC] is observed during winter. The map for winter (Figure S3) shows a large expanse of area with a 0.6 to 0.8 probability that covers southern Finland, European Russia, and the former USSR countries, Estonia, Latvia, Lithuania, Belarus, and Ukraine. There are smaller areas of 0.6 to 0.8 probabilities extending into the Czech Republic, Poland, and Hungary. The area of 0.8 to 1.0 probabilities is situated in southern Russia. Fires in Ukraine and European Russia coincide with the harvest of winter and spring grains [*Korontzi et al.*, 2006; *McCarty et al.*, 2012]. The summer map for 1964–1990 (Figure S7) is similar to Figure S2 as there are no discernable source regions. The map for winter 1964–1990 (Figure S5) shows the high-probability source region that are more focused in the European region of Russia but have lower probabilities (highest 0.6–0.8). Note that many of the trajectories that pass through the high-emission areas in the former USSR would also pass through the Kola Peninsula; however, the proximity of the Kola Peninsula to Kevo would preclude this region being highlighted by the PSCF analysis as air masses from the high Arctic reaching Kevo from the east would have low BC and would often also pass through the Kola Peninsula canceling out a high PSCF probability from this area.

4.3. Comparison of Measured [BC] With Emission and Model Simulations

4.3.1. Comparison of [BC] Trends With Emission Calculations

Novakov et al. [2003] estimated BC emissions from fossil fuel combustion from 1950 to 2000 for various countries including the United States (US), United Kingdom (UK), Germany (GER), and the former Soviet Union (USSR). The sum of the emissions for UK + GER + USSR is shown in Figure 8 (designated Novakov).

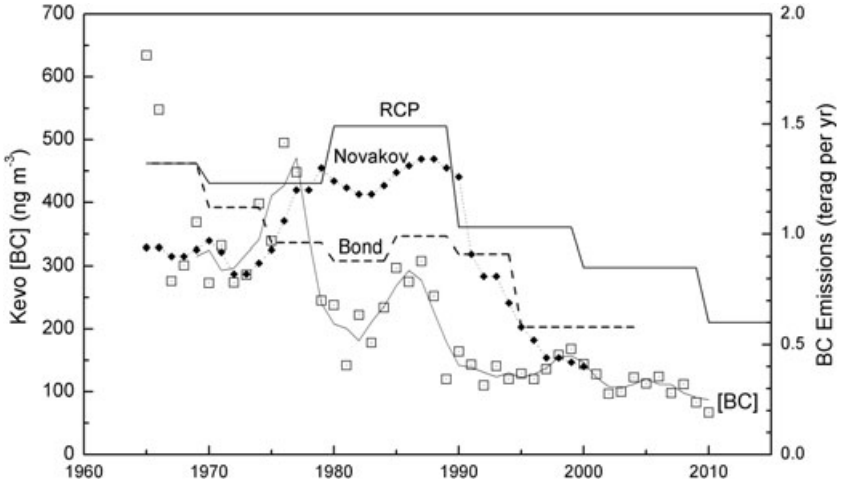

Figure 8. Time series plot of [BC] measured at Kevo, Finland, for 1965–2010 compared to selected BC emission estimates given below: Novakov = BC emissions for UK + GER + USSR [*Novakov et al*., 2003] Bond = BC emissions for OECD Europe + USSR [*Bond et al*., 2007] RCP = BC emissions for Europe + USSR [*Lamarque et al*., 2010; *Riahi et al*., 2011].

Bond et al. [2007] reported global historic BC fossil fuel and biofuel (FFBF) emission by regions averaged at 5 year intervals (http://www.hiwater.org/). The sum of the emissions for the former Soviet Union + Europe is shown in Figure 8 (designated as Bond). *Lamarque et al*. [2010] reported gridded FFBF emissions for every tenth year from 1960 to 2000 and designated as RCP. *Riahi et al*. [2011] extended these emissions to include 2005 and 2010. The summed emissions for USSR and Europe are shown as RCP in Figure 8. *Sharma et al*. [2013] reported annual BC emissions from fossil fuel combustion for Western Europe (WEUR), North America (NA), and the USSR for only a brief period covered by this study; (1990 to 2005), so they are not shown in Figure 8.

For all three inventories the European component of the emissions in the 1960s are ~0.5 Tg/yr and steadily decrease through the period. For the most part the structures in the emissions' profiles in Figure 8 are due to the USSR emissions. The Bond and RCP emissions are equal in the 1960s, but Novakov's is around 0.4 Tg lower. Around 1973 the Novakov emissions began to rapidly increase while the Bond emissions decrease in 1975. Owing to the 10 year reporting by RCP, no variation can be observed over this period. During the 1980s, the Novakov and RCP are distinctly elevated; around 1.3 Tg and 1.5 Tg, respectively. The Bond emissions remain around 0.9 Tg. In the 1990s the Novakov and RCP emissions greatly decrease but not so for the Bond emissions, which shows a large decrease in 1995. The emissions given in *Sharma et al*. [2013] also showed a large decrease around 1990 (not shown in Figure 8), and the authors linked it to the economic slowdown that was brought about by the collapse of the USSR. The Bond emissions miss the 1990 dropoff in USSR emissions. While none of the emission profiles in Figure 8 truly follow the [BC], the overall similarity in the patterns is encouraging suggesting that it is the USSR and European BC emissions that are controlling [BC] at Kevo. However, this simple comparison assumes equal contributions from the European and USSR emissions and does not account for the impact of transport or meteorology. The gridded RCP and Bond emissions are used to simulate historical [BC] using a model which incorporates both transport and removal processes in section 4.3.2.

4.3.2. Description of the OsloCTM3 Model

The measured [BC] are compared with modeled concentrations using the Oslo Chemical Transport Model (OsloCTM3) with different meteorological data and emission inventories. The OsloCTM3 is an updated version of the chemical transport model OsloCTM2 [*Myhre et al*., 2009; *Skeie et al*., 2011a]. The OsloCTM3 has a new transport scheme and updated wet scavenging scheme for large-scale rain [*Søvde et al*., 2012]. The model is driven by 3-hourly meteorological forecast data from the Integrated Forecast System model at the European Centre for Medium-Range Weather Forecasts. The BC module in OsloCTM3 is similar to the module used in OsloCTM2 [*Skeie et al*., 2011a]. It is a simple bulk scheme with hydrophobic and hydrophilic BC, where aging times are dependent on latitude and season based on simulation with OsloCTM2 and the M7 microphysical module [*Lund and Berntsen*, 2012]. Hydrophilic BC aerosols are removed in large-scale

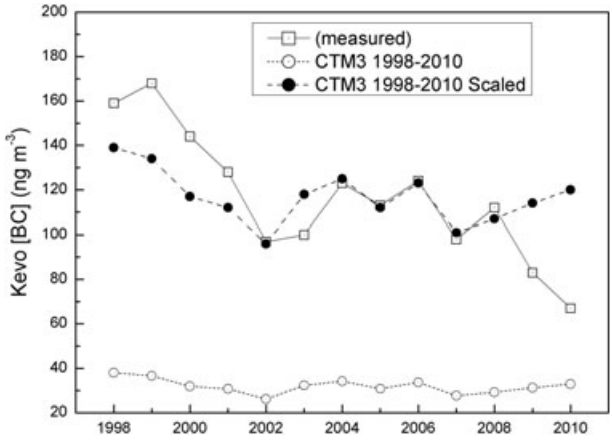

Figure 9. Annual mean [BC] from 1998 to 2010 plotted with CTM3 model simulated [BC] using year specific meteorological data as explained in the text. Simulations are also scaled by 3.7, so the ratio of the mean simulated [BC] to mean measured [BC] is 1.

precipitation; 100% scavenging is assumed in water clouds and 12% for ice clouds. For convective precipitation, 100% scavenging is assumed for both hydrophilic and hydrophobic aerosols. In the OsloCTM2 only hydrophilic BC were removed in convective precipitation [*Skeie et al*., 2011a]. The resolutions used here are T42 (approximately 2.8 × 2.8°) in the horizontal and 60 vertical levels from the surface to 0.1 hPa.

The meteorological data needed to drive the model are available only for 1997–2010, so to model the historic trend we need to select meteorological regimes that span transport conditions in the region. Thus, the model was first run from 1997 to 2010 with meteorological data specific for each year. Year 1997 is used as spin-up, so only results from 1998 to 2010 are shown in Figure 9. In this simulation the FFBF emissions are kept constant while the open biomass burning (BB) emissions correspond to the year simulated. For FFBF we used the 2005 emission data from the version 4a of the ECLIPSE (Evaluating the Climate and Air Quality Impacts of Shortlived Pollutants) emission data set (available from the Emissions of atmospheric Compounds & Compilation of Ancillary Data (http://eccad.sedoo.fr) database), and the BB emissions were from the Global Fire Emissions Database version 3.1 [*Van der Werf et al*., 2010].

4.3.3. Comparison of Model Results and Observations, 1997–2010

In the middle of the simulation period, the year to year trend closely follows the Kevo measurements (Figure 9). However, the absolute magnitude is severely underestimated, outside the range of uncertainties in the measurements (see section 3.1.1). In Figure 9, the modeled concentrations are also scaled by a factor of 3.7, so the average modeled and observed concentration over the 1998 to 2010 period are equal. The model under predicts the observations in all seasons, as seen in Figure 10 where monthly modeled and observed [BC] from 1998 to 2010 are compared. The model does not capture the large observed concentration during winter and spring, with the largest underestimation in spring by a factor of 5. It is known that global models fail to reproduce Arctic surface concentration [*Koch et al*., 2009; *Shindell et al*., 2008]. The OsloCTM2 was included in a multimodel study [*Lee et al*., 2013] which showed that the Oslo CTM2, like other models, fails to reproduce the seasonality in Arctic atmospheric [BC], due to a significant underestimation in winter and spring. The underestimation might be due to limitation in the emission inventories as

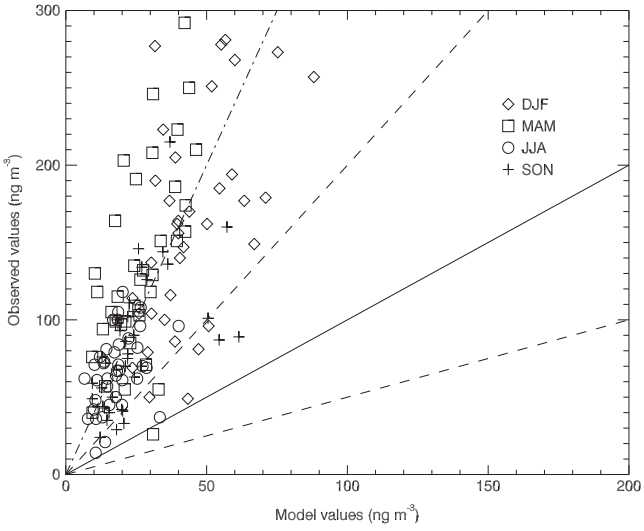

Figure 10. Scatterplot of monthly modeled and observed [BC] at Kevo for the period 1998 to 2010 (ng m^{-3}). The winter (DJF, December-January-February) values shown as diamond, spring (MAM, March-April-May) values as squares, summer (JJA, June-July-August) values as circles, and autumn (SON, September-October-November) values as crosses. The solid line shows a one-to-one correspondence, the dashed lines a factor of 2 difference between the model results and the observations and the dashed-dotted line 4 times larger values for the observations than model results.

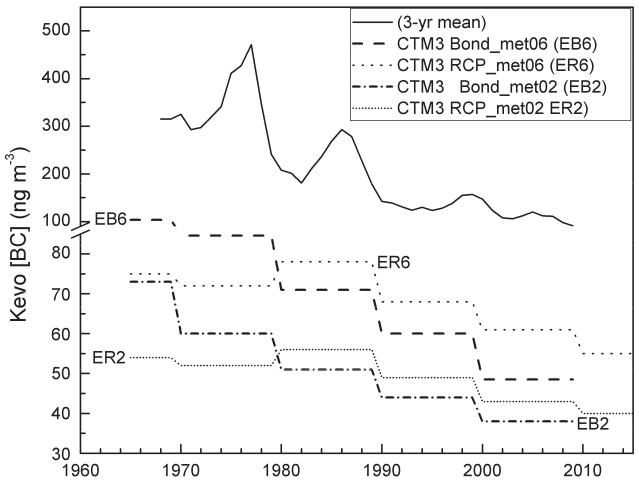

Figure 11. Time series plot of 3 years mean [BC] at Kevo, Finland, (Figure 5) and model simulated [BC] using OsloCTM3 model as explained in the text. The every 10 year values in the simulations are taken as averages over that decade.

well as uncertainties in the modeling. There might be missing BB sources during spring [*Skeie et al*., 2011a]. The simulation predicts that open BB contributed to only 1–8% of the annual mean concentration at Kevo for the period 1998–2010. There is also no seasonal variation in the FFBF emissions used in the model. *Stohl et al*. [2013] showed that including seasonal variation in domestic emissions (e.g., wood burning for heating) improved the modeled seasonal cycle in the Arctic. There are also large uncertainties related to the total emissions of BC [*Bond et al*., 2007]. In addition to emission uncertainties there are large uncertainties in the BC modeling, and especially wet removal of BC [*Vignati et al*., 2010; *Schwarz et al*., 2010]. Several studies point at wet removal as the key uncertainty in the modeling of the seasonal cycle of Arctic [BC] [*Garrett et al*., 2010, 2011; *Browse et al*., 2012; *Lee et al*., 2013; *Wang et al*., 2013].

In Figure 9 the downward trend in the observations for 1998–2010 is not captured by the model running with constant FFBF emissions suggesting that there is a downward trend in the FFBF emissions in regions influencing the surface concentration at Kevo. The elevated [BC] measured at Kevo in 1999 is also not captured by the model suggesting that the emissions from the Kola Peninsula are underestimated. As the lowest simulated FFBF [BC] occurred in 2002 and the highest in 2006, the meteorology during these years represents low and high BC transport conditions.

4.3.4. Comparison of Modeled and Observed Black Carbon Trends

To simulate the historical period (Figure 11), time slice simulations were performed with meteorological data for year 2002 and 2006 as discussed above. As noted above, BB emissions have a minor contribution to the annual [BC], so the data for 2002 and 2006 were used. Previous model studies show even lower contributions from BB to Arctic BC burden using a historical emission inventory for open BB [*Skeie et al*., 2011a]. For the FFBF emissions, two different historical inventories introduced in Figure 8 are used [*Bond et al*., 2007] every tenth year from 1960 to 2000 and RCP historical emissions every tenth year from 1960 to 2000 [*Lamarque et al*., 2010] in addition to RCP8.5 for 2005 and 2010 emissions [*Riahi et al.,* 2011].

The modeled trends are shown in Figure 11. The lowest values are for the simulations with year 2002 meteorology and the highest values using 2006 meteorology. The simulations with the RCP emissions show a slight increase from the 1970s to 1980s, as is also seen in the observed [BC] from around 1970 to 1978, however, stronger. The simulations using Bond emission data show a downward trend for the entire time period, with 1.0 and 1.2% yr^{-1} for the 1970–2000, 2002, and 2006 periods, respectively. Using the RCP emissions, the downward trend is 1.0% and 1.2% yr^{-1} between 1970 and 2010 for the 2002 and 2006 simulation, respectively. These values represent weaker trends compared to the observed decreasing trend of 1.8% yr^{-1} between ~1970 and 2010. The modeled trends are purely driven by changes in the emissions. There might be larger variability in the meteorological conditions than over the period 1998 to 2010. *Eckhardt et al.* [2003] showed that the North Atlantic Oscillation controls air pollution transport to the Arctic particularly in winter and spring. *Sharma et al.* [2013] investigated the impact of meteorology on simulated BC transport to the Arctic from 1990 to 2005. They found that changes in meteorology alone could not explain the observed trends, but it was reflected in the interannual variations in wintertime measurements at three Arctic sites (Alert, Barrow, and Ny Ålesund). The trends in wintertime BC from 1990 to 2005 at the sites were governed by changes in emissions in the northern midlatitude regions, but they also found that transport from Eurasia to the Arctic was much more frequent during 1990 to 1994 than 2001 to 2005 periods.

The results indicate that circulation changes can explain year to year variability, but the downward trend in the observations is mostly explained by emissions. It is also likely that the emission from wood burning for heating varies with the meteorological conditions. However, there is no seasonal variability in the emission inventories used in the domestic sector. Furthermore, the emissions are not linked to meteorological condition.

The same set of aging times is used throughout the historical simulations. The aging are dependent on sulfate concentration, which have declined over the past decades in the regions close to Kevo [e.g., *Skeie et al.* [2011b]]. This indicates that the lifetime of BC might be overestimated in the early time of the simulation and that the modeled declining trend should have been even slower.

There are large uncertainties in historical emission inventories. *Bond et al.* [2007] indicated a factor 2 uncertainty in present-day total global FFBF BC emissions but did not estimate uncertainty in the spatial distribution of the emissions or uncertainties in the rate of change in the emissions. As from the analysis in section 4.2 the main source regions for Kevo in the model is Europe and the former Soviet Union. In a 2006 OsloCTM2 simulation presented in *Skeie et al.* [2011a] the regional contribution to BC at Kevo was 56% from EU17, 22% from Russia and the former Soviet Union, and 17% from the rest of Europe.

The comparison between OsloCTM3 model results for Kevo and the observed concentration indicate that the historical emissions in Europe, Russia, and former Soviet Union need revision for better representation of historical [BC] trends in the model. Also, the current emissions at high latitudes should be further investigated. *Stohl et al.* [2013] found that gas flaring included in the ECLIPSE emission data contributes to 42% of the annual mean Arctic surface concentration. Although the ECLIPSE emissions better represent high-latitude emissions of BC than other inventories, the results by *Stohl et al.* [2013] indicate that the high-latitude emissions are still underestimated. A model study by *Sand et al.* [2013] found that BC emitted within the Arctic has an almost 5 times larger Arctic surface temperature response (per unit of emitted mass) compared to emissions at midlatitudes highlighting the importance of good representation of high-latitude BC emissions.

5. Summary and Conclusions

Concentrations of BC were determined in weekly aerosol samples collected at Kevo, Finland, on Whatman 42 or glass fiber filters from 1964 to 2010. Measurements were made using optical and thermal optical methods. The highest annual mean concentrations were observed in 1965–1966, 671 ng m^{-3} (although local wood burning may have had an impact at this time). Concentrations decreased sharply, averaging around ~300 ng m^{-3} for the 1970–1980, ~250 ng m^{-3} for 1981–1990, ~140 ng $m^{-3}$for the 1991–2000, and ~100 ng m^{-3} for the 2001–2010 periods. Between 1971 and 2010 BC concentrations decreased by 78% or 1.8% yr^{-1}. The highest concentrations were observed in winter, moderate in autumn and spring, and the lowest in summer. Model calculations using the OsloCTM3 yields BC concentration values ~4 times lower than those observed at Kevo between 1998 and 2010; however, the time trend is reasonably reproduced. There are limitations in global models to reproduce Arctic surface concentration, but the comparison of model and observations might also indicate that the emissions in source regions are too low (particularly emissions in the former Soviet Union). Also, the modeled historical trend is underestimated. The data presented in this study provide the longest record of *directly* measured [BC] in the Arctic. It can be used to improve historical emission inventories for the regions affecting the surface concentration in the European Arctic. Revised emission inventories will impact the radiative forcing trend calculations, including the snow albedo effect, and be important for detection and attribution of climate change studies.

Acknowledgments
We thank Tim Hoffman of the Wadsworth Center machine shop for his assistance in producing the high-precision masks used for the GF filter analysis. This work was supported in part by the National Science Foundation under grants AGS-1007261, AGS-1063323 (HRI-Albany), and AGS-1007329 (Clarkson University). R.B. Skeie was funded by the Norwegian Research Council through the project SLAC (Short Lived Atmospheric Components) and from the European Union Seventh Framework Programme (FP7/2007–2013) under grant agreement 282688—ECLIPSE.

References

Ahmed, T., V. A. Dutkiewicz, A. Shareef, G. Tuncel, S. Tuncel, and L. Husain (2009), Measurement of black carbon (BC) by an optical method and a thermal-optical method: Intercomparison for four sites, *Atmos. Environ.*, *43*, 6305–6311.

Begum, B. A., A. Hossain, G. Saroar, S. K. Biswas, M. Nasiruddin, N. Nahar, Z. Chowdury, and P. K. Hopke (2011), Carbonaceous materials in the airborne particulate matter of Dhaka, *Asian J. Atmos. Environ.*, *5–4*, 237–246.

Birch, M. E., and R. A. Cary (1996), Elemental carbon based for monitoring occupational exposures to particulate diesel exhaust, *Aerosol Sci. Technol.*, *25*, 221–241.

Bodhaine, B. (1989), Barrow surface aerosol: 1976–1986, *Atmos. Environ.*, *23*(11), 2357–2369.

Bond, T. C., E. Bhardwaj, R. Dong, R. Jogani, S. K. Jung, D. Roden, D. G. Street, and N. M. Trautmann (2007), Historical emissions of black and organic carbon aerosols from energy-related combustion, 1850–2000, *Global Biogeochem. Cycles*, *21*, GB2018, doi:10.1029/2006GB002840.

Bond, T. C., et al. (2013), Bounding the role of black carbon in the climate system: A scientific assessment, *J. Geophys. Res. Atmos.*, *118*, 5380–5552, doi:10.1002/jgrd.50171.
Boyd, R., S.-J. Barnes, P. De Caritat, V. A. Chekushin, V. A. Melezhik, C. Reimann, and M. L. Zientek (2009), Emissions from the copper-nickel industry on the Kola Peninsula and at Noril'sk, Russia, *Atmos. Environ.*, *43*, 1474–1480.
Browse, J., K. S. Carslaw, S. R. Arnold, K. Pringle, and O. Boucher (2012), The scavenging processes controlling the seasonal cycle in Arctic sulphate and black carbon aerosol, *Atmos. Chem. Phys.*, *12*, 6775–6798, doi:10.5194/acp-12-6775-2012.
Cheng, M. D., P. K. Hopke, L. Barrie, A. Rippe, M. Olson, and S. Landsberger (1993), Qualitative determination of source regions of aerosol in Canadian high Arctic, *Environ. Sci. Technol.*, *27*, 2063–2071.
Chow, J. C., J. G. Watson, L. C. Pritchett, W. R. Pierson, C. A. Frazier, and R. G. Purcell (1993), The DRI thermal/optical reflectance carbon analysis system: Description, evaluation and applications in U.S. air quality studies, *Atmos. Environ.*, *27A*, 1185–1201.
Chow, J. C., J. G. Watson, D. Crow, D. H. Lowenthal, and T. Merrifield (2001), Comparison of IMPROVE and NIOSH carbon measurements, *Aerosol Sci. Technol.*, *34*, 23–34.
Dockery, D. W., C. A. Pope III, X. Xu, J. D. Spengler, J. H. Ware, E. Martha, M. E. Fay, B. G. Ferris Jr., and F. E. Speitzer (1993), An association between air pollution and mortality in six U.S. cities, *N. Engl. J. Med.*, *329*, 1753–1759.
Draxler, R. R., and G. D. Hess (1998), An overview of the HYSPLIT_4 modeling system for trajectories, dispersion and deposition, *Aust. Meteorol. Mag.*, *47*, 295–308.
Eckhardt, S., A. Stohl, S. Beirle, N. Spichtinger, P. James, C. Forster, C. Junker, T. Wagner, U. Platt, and S. G. Jennings (2003), The North Atlantic Oscillation controls air pollution transport to the Arctic, *Atmos. Chem. Phys.*, *3*, 1769–1778.
Eleftheriadis, K., S. Vratolis, and S. Nyeki (2009), Aerosol black carbon in the European Arcric: Measurements at Zeppelin station, Ny Ålesund, Svalbard from 1998–2007, *Geophys. Res. Lett.*, *36*, L02809, doi:10.1029/2008GL035741.
Fan, A., P. K. Hopke, T. Raunemaa, M. Oblad, and J. M. Pacyna (1994), A study on the potential sources of air pollutants observed at Tjorn, Sweden, *Environ. Sci. Pollut. Res.*, *2*, 107–115.
Flanner, M. G., C. S. Zender, P. G. Hess, N. M. Mahowald, T. H. Painter, V. Ramanathan, and P. J. Rasch (2009), Springtime warming and reduced snow cover from carbonaceous particles, *Atmos. Chem. Phys.*, *9*, 2481–2497.
Forastiere, F. (2004), Fine particles and lung cancer, *Occup. Environ. Med.*, *61*, 797–798, doi:10.1136/oem.2004.014290.
Garrett, T. J., C. Zhao, and P. C. Novelli (2010), Assessing the relative contributions of transport efficiency and scavenging to seasonal variability in Arctic aerosol, *Tellus, Ser. B*, *62*, 190–196, doi:10.1111/j.1600-0889.2010.00453.x.
Garrett, T. J., S. Brattström, S. Sharma, D. E. J. Worthy, and P. Novelli (2011), The role of scavenging in the seasonal transport of black carbon and sulfate to the Arctic, *Geophys. Res. Lett.*, *38*, L16805, doi:10.1029/2011GL048221.
Gong, S. L., T. L. Zhao, S. Sharma, D. Toom-Sauntry, D. Lavoué, X. B. Zhang, W. R. Leaitch, and L. A. Barrie (2010), Identification of trends and interannual variability of sulfate and black carbon in the Canadian high Arctic: 1981–2007, *J. Geophys. Res.*, *115*, D07305, doi:10.1029/2009JD012943.
Hansen, J., and L. Nazarenko (2004), Soot climate forcing via snow and ice albedos, *Proc. Natl. Acad. Sci. U.S.A.*, *101*, 423–428.
Haywood, J. M., and K. P. Shine (1995), The effect of anthropogenic sulfate and soot aerosols on the clear sky planetary budget, *Geophys. Res. Lett.*, *22*, 603–606, doi:10.1029/95GL00075.
Husain, L., A. J. Khan, T. Ahmed, K. Swami, A. Bari, J. S. Webber, and J. Li (2008), Trends in atmospheric elemental carbon concentrations from 1835 to 2005, *J. Geophys. Res.*, *113*, D13102, doi:10.1029/2007JD009398.
Husain, L., V. A. Dutkiewicz, and W. Maenhaut (2011), Variation in aerosol black carbon in NY Alesund, Spitsbergen, Norway, from 1991 to 2004, The Arctic as a Messenger for Global Processes- Climate Change and Pollution, Copenhagen, Denmark, May 3–6.
Iversen, T., and E. Joranger (1985), Arctic air pollution and large scale atmospheric flows, *Atmos. Environ.*, *19*, 2099–2108.
Jacobson, M. Z. (2002), Control of fossil fuel particulate black carbon and organic matter, possibly the most effective method of slowing global warming, *J. Geophys. Res., 107*(D19), 4410, doi:10.1029/2001JD001376.
Khan, A. J., J. Li, and L. Husain (2006), Atmospheric transport of elemental carbon, *J. Geophys. Res.*, *111*, D04303, doi:10.1029/2005JD006505.
Koch, D., et al. (2009), Evaluation of black carbon estimations in global aerosol models, *Atmos. Chem. Phys.*, *9*(22), 9001–9026.
Korontzi, S., J. McCarty, T. Loboda, S. Kumar, and C. Justice (2006), Global distribution of agricultural fires in croplands from 3 years of Moderate Resolution Imaging Spectroradiometer (MODIS) data, *Global Biogeochem. Cycles*, *20*, GB2021, doi:10.1029/2005GB002529.
Laing, J. R., P. K. Hopke, E. F. Hopke, L. Husain, V. A. Dutkiewicz, J. Paatero, and Y. Viisanen (2013), Long-term trends of biogenic sulfur aerosol and its relationship with sea surface temperature in Arctic Finland, *J. Geophys. Res. Atmos.*, *118*, 11,770–11,776, doi:10.1002/2013JD020384.
Laing, J. R., P. K. Hopke, E. F. Hopke, L. Husain, V. A. Dutkiewicz, J. Paatero, and Y. Viisanen (2014a), Long-term particle measurements in Finnish Arctic: Part I—Chemical composition and trace metal solubilities, *Atmos. Environ.*, *88*, 275–284, doi:10.1016/j.atmosenv.2014.03.002.
Laing, J. R., P. K. Hopke, E. F. Hopke, L. Husain, V. A. Dutkiewicz, J. Paatero, and Y. Viisanen (2014b), Long-term particle measurements in Finnish Arctic: Part II—Trend analysis and source location identification, *Atmos. Environ.*, *88*, 285–296, doi:10.1016/j.atmosenv.2014.01.015.
Lamarque, J. F., et al. (2010), Historical (1850–2000) gridded anthropogenic and biomass burning emissions of reactive gases and aerosols: Methodology and application, *Atmos. Chem. Phys.*, *10*, 7017–7039, doi:10.5194/acp-10-7017-2010.
Lee, Y. H., et al. (2013), Evaluation of preindustrial to present-day black carbon and its albedo forcing from Atmospheric Chemistry and Climate Model Intercomparison Project (ACCMIP), *Atmos. Chem. Phys.*, *13*, 2607–2634, doi:10.5194/acp-13-2607-2013.
Li, J., A. J. Khan, and L. Husain (2002), A technique for determination of black carbon in cellulose filters, *Atmos. Environ.*, *36*, 4699–4704.
Liousse, C., H. Cachier, and S. G. Jennings (1993), Optical and thermal measurements of black carbon aerosol content in different environments: Variation of the specific attenuation cross section, sigma (σ), *Atmos. Environ.*, *27A*, 1203–1211.
Lund, M. T., and T. Berntsen (2012), Parameterization of black carbon aging in the OsloCTM2 and implications for regional transport to the Arctic, *Atmos. Chem. Phys.*, *12*, 6999–7014, doi:10.5194/acp-12-6999-2012.
McCarty, J. L., E. A. Ellicott, V. Romanenkov, D. Rukhovitch, and P. Koroleva (2012), Multi-year black carbon emissions from cropland burning in the Russian Federation, *Atmos. Environ.*, *63*, 223–238.
McConnell, J. R., R. Edwards, G. L. Kok, M. G. Flanner, C. S. Zender, E. S. Saltzman, J. R. Banta, D. R. Pasteris, M. M. Carter, and J. D. W. Kahl (2007), 20th-century industrial black carbon emissions altered Arctic climate forcing, *Science*, *317*(5843), 1381–1384.
Myhre, G., et al. (2009), Modelled radiative forcing of the direct aerosol effect with multi-observation evaluation, *Atmos. Chem. Phys.*, *9*, 1365–1392, doi:10.5194/acp-9-1365-2009.
National Institute for Occupational Safety and Health (NIOSH) (1996), Elemental carbon (diesel exhaust), in *NIOSH Manual of Analytical Methods*, National Institute of Occupational Safety and Health, Cincinnati, Ohio.

Novakov, T., V. Ramanathan, J. E. Hansen, T. W. Kirchstetter, M. Sato, J. E. Sinton, and J. A. Sathaye (2003), Large historical changes of fossil-fuel black carbon aerosols, *Geophys. Res. Lett., 30*(6), 1324, doi:10.1029/2002GL016345.
Ogren, J. A., and R. J. Charlson (1983), Elemental carbon in the atmosphere: Cycle and lifetime, *Tellus, Ser. B, 35*, 241–254.
Paatero, J., R. Mattsson, and J. Hatakka (1994a), *Measurements of Airborne Radioactivity in Finland, 1983–1990 and Applications to Air Quality Studies*, Publications on Air Quality No. 17, Finnish Meteorological Institute, Helsinki, Finland.
Paatero, J., J. Hatakka, R. Mattsson, and I. Lehtinen (1994b), A comprehensive station for monitoring atmospheric Radioactivity, *Radiat. Prot. Dosim., 54*, 33–39.
Park, S. S., A. D. A. Hansen, and S. Y. Cho (2010), Measurement of real time black carbon for investigating spot loading effects of aethalometer data, *Atmos. Environ., 44*, 1449–1455, doi:10.1016/J.atmosenv.2010.01.025.
Petzold, A., C. Kopp, and R. Niessner (1997), The dependence of the specific attenuation cross section on black carbon mass fraction and particle size, *Atmos. Environ., 31*, 661–672.
Pirinen, P., H. Simola, J. Aalto, J.-P. Kaukoranta, P. Karlsson, and R. Ruuhela (2012), *Climatological Statistics of Finland 1981–2010*, Reports 2012:1, Finnish Meteorological Institute, Helsinki.
Polissar, A. V., P. K. Hopke, P. Paatero, Y. J. Kaufmann, D. K. Hall, B. A. Bodhaine, E. G. Dutton, and J. M. Harris (1999), The aerosol at Barrow, Alaska: Long-term trends and source locations, *Atmos. Environ., 33*, 2441–2458.
Polissar, A. V., P. K. Hopke, and J. M. Harris (2001), Source regions for atmospheric aerosol measured at Barrow, Alaska, *Environ. Sci. Technol., 35*, 4214–4226.
Pope, C. A., R. T. Burnett, M. J. Thun, E. E. Calle, D. Krewski, K. Ito, and G. D. Thurston (2002), Lung cancer, cardiopulmonary mortality, and long-term exposure to fine particulate air pollution, *JAMA, J. Am. Med. Assoc., 287*(9), 1132–1141.
Raatz, W. E., and G. E. Shaw (1984), Long-range tropospheric transport of pollution aerosols into the Alaskan Arctic, *J. Clim. Appl. Meteorol., 23*, 1052–1064.
Ramanathan, V., and G. Carmichael (2008), Global and regional climate changes due to black carbon, *Nat. Geosci., 1*, 221–227.
Riahi, K., S. Rao, V. Krey, C. Cho, V. Chirkov, G. Fischer, G. Kindermann, N. Nakicenovic, and P. Rafaj (2011), RCP 8.5—A scenario of comparatively high greenhouse gas emissions, *Clim. Change, 109*, 33–57, doi:10.1007/s10584-011-0149-y.
Rom, W. N., and J. M. Samet (2006), Small particles with big effects, *Am. J. Respir. Crit. Care Med., 173*, 365–369.
Salako, G. O., et al. (2012), Exploring the variation between EC and BC in a variety of locations, *Aerosol Air Qual. Res., 12*, 1–7.
Sand, M., T. K. Berntsen, O. Seland, and J. E. Kristjansson (2013), Arctic surface temperature change to emissions of black carbon within Arctic and midlatitudes, *J. Geophys. Res. Atmos., 118*, 7788–7798, doi:10.1002/jgrd.50613.
Schmid, O., P. Artaxo, W. P. Arnott, D. Chand, L. V. Gatti, G. P. Frank, A. Hoffer, M. Schnaiter, and M. O. Andreae (2006), Spectral light absorption by ambient aerosols influenced by biomass burning in the Amazon Basin. I: Comparison and field calibration of absorption measurement techniques, *Atmos. Chem. Phys., 6*, 3443–3462, doi:10.5194/acp-6-3443-2006.
Schwarz, J. P., J. R. Spackman, R. S. Gao, L. A. Watts, P. Stier, M. Schulz, S. M. Davis, S. C. Wofsy, and D. W. Fahey (2010), Global-scale black carbon profiles observed in the remote atmosphere and compared to models, *Geophys. Res. Lett., 37*, L18812, doi:10.1029/2010GL044372.
Sharma, S., D. Lavoue, H. Cachier, L. Barrie, and S. Gong (2004), Long-term trends of the black carbon concentrations in the Canadian Arctic, *J. Geophys. Res., 109*, D15203, doi:10.1029/2003JD004331.
Sharma, S., M. Ishizawa, D. Chan, D. Lavoué, E. Andrews, K. Eleftheriadis, and S. Maksyutov (2013), 16 year simulation of Arctic black carbon: Transport, source contributions and sensitivity analysis of deposition, *J. Geophys. Res. Atmos., 118*, 943–964, doi:10.1029/2012JD017774.
Shaw, G. E. (1995), The Arctic haze phenomenon, *Bull. Am. Meteorol. Soc., 76*, 2403–2413.
Shindell, D. T., et al. (2008), A multi-model assessment of pollution transport to the Arctic, *Atmos. Chem. Phys., 8*(17), 5353–5372.
Skeie, R. B., T. K. Bernsten, G. Myhre, C. A. Pedersen, J. Ström, S. Gerland, and J. A. Ogren (2011a), Black carbon in the atmosphere and snow, from pre-industrial times until present, *Atmos. Chem. Phys., 11*, 6809–6836.
Skeie, R. B., T. K. Bernsten, G. Myhre, K. Tanaka, M. M. Kvalevåg, and C. R. Hoyle (2011b), Anthropogenic radiative forcing times series from pre-industrial time until 2010, *Atmos. Chem. Phys., 11*, 11,827–11,857.
Søvde, O. A., M. J. Prather, I. S. A. Isaksen, T. K. Berntsen, F. Stordal, X. Zhu, C. D. Holmes, and J. Hsu (2012), The chemical transport model Oslo CTM3, *Geosci. Model Dev., 5*, 1441–1469, doi:10.5194/gmd-5-1441-2012.
Stohl, A., Z. Klimont, S. Eckhardt, K. Kupiainen, V. P. Shevchenko, V. M. Kopeikin, and A. N. Novigatsky (2013), Black carbon in the Arctic: The underestimated role of gas flaring and residential combustion emissions, *Atmos. Chem. Phys., 13*, 8833–8855, doi:10.5194/acp-13-8833-2013.
Tuovinen, J. P., T. Laurila, H. Lättilä, A. Ryaboshapko, P. Brukhanov, and S. Korolev (1993), Impact of the sulphur dioxide sources in the Kola Peninsula on air quality in northernmost Europe, *Atmos. Environ., 27A*, 1379–1395.
Van der Werf, G. R., J. T. Randerson, L. Giglio, G. J. Collatz, M. Mu, P. S. Kasibhatla, D. C. Morton, R. S. DeFries, Y. Jin, and T. T. van Leeuwen (2010), Global fire emissions and the contribution of deforestation, savanna, forest, agricultural, and peat fires (1997–2009), *Atmos. Chem. Phys., 10*, 11,707–11,735, doi:10.5194/acp-10-11707-2010.
Vignati, E., M. Karl, M. Krol, J. Wilson, P. Stier, and F. Cavalli (2010), Sources of uncertainties in modeling black carbon at the global scale, *Atmos. Chem. Phys., 10*(6), 2595–2611.
Viidanoja, J., M. Sillanpää, J. Laakia, V.-M. H. Kerminen, R. Illamo, P. Aarnio, and T. Koskentalo (2002), Organic and black carbon in $PM_{2.5}$ and PM_{10}: 1 year data from an urban site in Helsinki, Finland, *Atmos. Environ., 36*, 3183–3193.
Virkkula, A., T. Makela, R. Hillamo, T. Yli-Tuomi, A. Hirsikko, K. Hameri, and I. K. Koponen (2007), A simple procedure for correcting loading effects of aethalometer, *J. Air Waste Manage. Assoc., 57*, 1214–1222.
Wang, H., R. C. Easter, P. J. Rasch, M. Wang, X. Liu, S. J. Ghan, Y. Qian, J. H. Yoon, P. L. Ma, and V. Vinoj (2013), Sensitivity of remote aerosol distributions to representation of cloud–aerosol interactions in a global climate model, *Geosci. Model Dev., 6*, 765–782, doi:10.5194/gmd-6-765-2013.
Warren, S. G., and W. J. Wiscombe (1980), A model for the spectral albedo of snow. II. Snow containing atmospheric aerosols, *J. Atmos. Sci., 37*, 2734–2745.
Weingartner, E., H. Saathoff, M. Schnaiter, N. Streit, B. Bitnar, and U. Baltensperger (2003), Absorption of light by soot particles: Determination of the absorption coefficient by means of aethalometer, *J. Aerosol Sci., 34*, 1445–1463.
Yli-Tuomi, T., P. K. Hopke, P. Paatero, M. S. Basunia, S. Landsberger, Y. Viisanen, and J. Paatero (2003), Atmospheric aerosol over Finnish Arctic: Source analysis by the multilinear engine and the potential source contribution function, *Atmos. Environ., 37*, 81–4392.